VSP

Advanced Composite Materials 18 (2009) 381–394

ADVANCED COMPOSITE MATERIALS
www.brill.nl/acm

Centrifugal Infiltration Process of Fibrous Tubular Preform by Al–Cu Alloy

Yanhong Li, Kai Wang, Yongkang Su and Guoxin Hu *

School of Mechanical and Power Engineering, Shanghai Jiaotong University, Shanghai 200240, China

Received 21 September 2008; accepted 2 December 2008

Abstract

The kinetics of centrifugal infiltration of fibrous tubular preform is built theoretically, and simulations are conducted to study the effects of various casting conditions on infiltration kinetics and macrosegregation by combining with the energy, mass and kinetic equations. A similarity way is used to simplify the one-dimensional model and the parameter is ascertained by an iterative method. The results indicate that the increase of superheat, initial preform temperature, porosity tends to enlarge the remelting region and decrease copper solute concentration at the infiltration front. Higher angular velocity leads to smaller remelting region and solute concentration at the tip. The pressure in the infiltrated region increase significantly when the angular velocity is much higher, which requires a stronger preform. It is observed that the pressure distribution is mainly determined by the angular velocity, and the macrosegregation in the centrifugal casting is greatly dependent on the superheat of inlet metal matrix, initial temperature and porosity of the preform, and the angular velocity.

Keywords

Metal matrix composites, centrifugal infiltration, simulation, porous preform, macrosegregation, Al-4.5 wt% Cu

Nomenclature

c specific heat capacity (J/Kg/K)

C solute concentration

d_f average diameter of fiber (m)

f volume fraction

k_0 equilibrium partial ratio

* To whom correspondence should be addressed. E-mail: hugx@sjtu.edu.cn
Edited by the KSCM

DOI:10.1163/156855108X399983

K preform permeability

m_L liquidus slope (K/wt%)

P pressure (Pa)

r radius (m)

S sectional area of the preform (m^2)

t time (s)

T temperature (K)

u radial superficial velocity (m/s)

V volume fraction

Greek

ΔH latent heat of phase change (J/Kg)

γ surface energy of the molten metal (Pa m)

θ_c contact angle (°)

λ thermal conductivity (W/m/K)

ρ density (kg/m^3)

μ dynamic viscosity (Pa s)

ϕ porosity

ω angular velocity (rad/s)

Subscripts

av average

c element of composite

e eutectic

f fiber

L liquid

m metal

p preform

s solid

SE solid eutectic metal

1. Introduction

Centrifugal infiltration processing method is one of the pressure casting used to manufacture metal matrix composites [1–3]. The infiltration process is in a centrifugal force field, which generates adequate pressure and makes the molten alloy possible to infiltrate a porous preform. Centrifugal casting method is suitable to be applied in manufacturing wear-resisting and corrosion-resisting sleeve or ring parts, and provides an extensive application prospective in commercial field [4].

Study of the fluid flow of the molten media and heat, mass transfer in the porous preform has important significance for casting technology design and improving the physical property of the products. Nishida [5] discussed the infiltration kinetics of pure molten metal in fibrous preforms by centrifugal force. Correlated equations of threshold pressure, infiltration rate, and pressure distribution have been analyzed theoretically. Hu *et al.* [6] presented a one dimensional model and the numerical results of the transient solidification and remelting by using the pure metal Al infiltrated through a preform in a centrifugal force field. For the case of infiltrating by an alloy, however, few researches have been published on the infiltration kinetics of molten alloy in a fibrous preform in the centrifugal force field.

In this paper, solidification and remelting of a binary hypoeutectic alloy are analyzed under a unidirectional infiltration of a fibrous tubular preform by centrifugal force. The infiltration kinetics is derived firstly to describe the infiltration of Al-4.5 wt% Cu into the Al_2O_3 porous preform. By combining the kinetic equations with the energy and mass equations, the effect of different operating parameters on the infiltration kinetics and solidification are investigated in detail. The average copper concentration, temperature, solid volume fraction, and pressure distribution profiles are presented for the prediction of the centrifugal force casting.

2. Model Formulation

Figure 1 is the schematic description of this physical model. Al-4.5 wt% Cu is used as the molten alloy, and the porous tubular preform is made of Al_2O_3 reinforcement. Region 1 is the mushy region where solid and liquid alloy coexist. Remelting region 2 is the region all of liquid metal in the case that inlet alloy is superheat ($T_{m,in} > T_m$). Region 3 is the uninfiltrated region. If the initial preform temperature is below the eutectic temperature of the alloy ($T_{p,0} < T_e$), it may have region 4 where solid metal is the eutectic alloy. $r_0, r_m(t)$ are locations of the inner surface of the molten metal at the initial time, and at time t, r_1, r_2 are the inner and outer boundary locations of the preform. r_s, r_e are the positions of the boundaries between region 2 and 1, region 1 and 4, and r_f is the location of infiltration front.

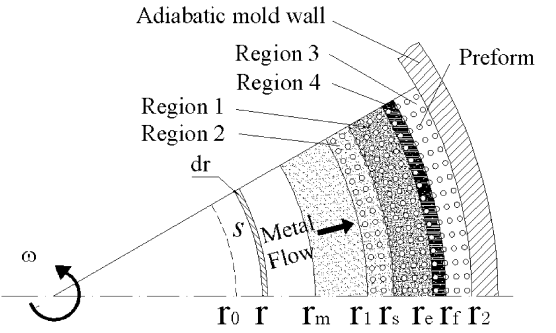

Figure 1. Schematic of infiltration processing of fibrous tubular preform by centrifugal casting.

2.1. Infiltration Kinetics

Darcy's law is used to describe the molten alloy flowing through the porous preform along the radius direction:

$$\frac{\partial P(r,t)}{\partial r} = -\frac{\mu u(r,t)}{K} + \rho_{\mathrm{m}}\omega^2 r. \tag{1}$$

Where K is the permeability related to porosity of the preform, and Happel's equation [5] is applied to obtain the value of K:

$$K = \frac{d_{\mathrm{sf}}^2}{32V_{\mathrm{sf}}}\left(-\ln V_{\mathrm{sf}} + \frac{V_{\mathrm{sf}}^2 - 1}{V_{\mathrm{sf}}^2 + 1}\right). \tag{2}$$

The threshold pressure P_{c} is given as following [5]:

$$P_{\mathrm{c}} = -\frac{4\gamma V_{\mathrm{sf}}\cos\theta_{\mathrm{c}}}{d_{\mathrm{sf}}(1 - V_{\mathrm{sf}})}, \tag{3}$$

where d_{sf} is the average diameter of the fiber, V_{sf} is the solid volume fraction of the preform, and $V_{\mathrm{sf}} = V_{\mathrm{f}} + V_{\mathrm{m}} f_{\mathrm{s}}$, $d_{\mathrm{sf}} = d_{\mathrm{f}}(V_{\mathrm{sf}}/V_{\mathrm{f}})^{1/2}$.

As it derived by Nishida [5], micro region from r to $r + dr$ is chosen to calculate the centrifugal force, and the pressure at the position r_1 could be given by:

$$P_1(t) = \frac{1}{3r_1}\rho_{\mathrm{m}}\omega^2\left(r_1^3 - (r_0^2 + \phi((r_{\mathrm{f}}(t))^2 - r_1^2))^{3/2}\right). \tag{4}$$

The relationship between the superficial velocity $u(r,t)$ and the radius r could be derived by the continuity equation:

$$\frac{\rho_{\mathrm{m}}}{r}\frac{\partial(ru(r,t))}{\partial r} = 0. \tag{5}$$

The following relationship is obtained from above equation: $ru(r,t) = B(t)$. The assumptions are given that the density and viscosity of the molten alloy are independent of t, but the permeability K is not a constant among different regions. Three cases are discussed for the appearance of different regions, which is caused by the different inlet metal temperature and the initial preform temperature. Case 1

only appears region 2; case 2 appears region 2 and 1; case 3 appears region 2, 1, and 4. All these three cases has region 3 of course. In region 1, the permeability K is different everywhere for the different V_{sf} in (2). The method using an average permeability derived by the preliminary calculation results is adopted to describe region 1. So, in region 2: $V_{sf} = V_f$, $K = K_1 =$ constant. In region 1: $f_s = f_{av}$, $K = K_2$. In region 4: $f_s = f_{SE}$, $K = K_3$.

The pressure at the position r is derived by the integration of Darcy's law. The equations in different regions are given as follows:

Region 2:

$$P(r,t) = P_1(t) - \frac{\mu B(t)}{K_1} \ln \frac{r}{r_1} + \frac{1}{2}\rho_m \omega^2 (r^2 - r_1^2). \tag{6}$$

Region 1:

$$P(r,t) = P_1(t) - \mu B(t)\left(\frac{1}{K_1} \ln \frac{r_s}{r_1} + \frac{1}{K_2} \ln \frac{r}{r_s}\right) + \frac{1}{2}\rho_m \omega^2 (r^2 - r_1^2). \tag{7}$$

Region 4:

$$P(r,t) = P_1(t) - \mu B(t)\left(\frac{1}{K_1} \ln \frac{r_s}{r_1} + \frac{1}{K_2} \ln \frac{r_e}{r_s} + \frac{1}{K_3} \ln \frac{r}{r_e}\right) + \frac{1}{2}\rho_m \omega^2 (r^2 - r_1^2). \tag{8}$$

$P_1(t)$ could be derived by putting $r = r_f(t)$ in the above equations, and the pressure $P(r,t)$ at $r_f(t)$ is the threshold pressure P_c. Then, the value of $P_1(t)$ is given in the following equations in different cases.

Case 1:

$$P_1(t) = P_c + \mu B(t) \frac{1}{K_1} \ln \frac{r_f}{r_1} - \frac{1}{2}\rho_m \omega^2 (r_f^2 - r_1^2). \tag{9}$$

Case 2:

$$P_1(t) = P_c + \mu B(t)\left(\frac{1}{K_1} \ln \frac{r_s}{r_1} + \frac{1}{K_2} \ln \frac{r_f}{r_s}\right) - \frac{1}{2}\rho_m \omega^2 (r_f^2 - r_1^2). \tag{10}$$

Case 3:

$$P_1(t) = P_c + \mu B(t)\left(\frac{1}{K_1} \ln \frac{r_s}{r_1} + \frac{1}{K_2} \ln \frac{r_e}{r_s} + \frac{1}{K_3} \ln \frac{r_f}{r_e}\right) - \frac{1}{2}\rho_m \omega^2 (r_f^2 - r_1^2). \tag{11}$$

From the relationship between $r_f(t)$ and $r_m(t)$, the relationship between the superficial velocity and the velocity of the infiltration front can be derived as following:

$$\frac{dr_f(t)}{dt} = \frac{u(t)}{\phi}. \tag{12}$$

By using (4) and (9)–(11), (12) can be rewritten as follows for different cases.

Case 1:

$$\mathrm{d}t = \frac{(\phi\mu r_\mathrm{f}/K_1)\ln r_\mathrm{f}/r_1}{P_1(t) - P_\mathrm{c} + 1/2\rho_\mathrm{m}\omega^2(r_\mathrm{f}^2 - r_1^2)}\,\mathrm{d}r_\mathrm{f}(t). \tag{13}$$

Case 2:

$$\mathrm{d}t = \frac{\phi\mu r_\mathrm{f}}{P_1(t) - P_\mathrm{c} + 1/2\rho_\mathrm{m}\omega^2(r_\mathrm{f}^2 - r_1^2)}\left(\frac{1}{K_1}\ln\frac{r_\mathrm{s}}{r_1} + \frac{1}{K_2}\ln\frac{r_\mathrm{f}}{r_\mathrm{s}}\right)\mathrm{d}r_\mathrm{f}(t). \tag{14}$$

Case 3:

$$\mathrm{d}t = \frac{\phi\mu r_\mathrm{f}}{P_1(t) - P_\mathrm{c} + 1/2\rho_\mathrm{m}\omega^2(r_\mathrm{f}^2 - r_1^2)}\left(\frac{1}{K_1}\ln\frac{r_\mathrm{s}}{r_1} + \frac{1}{K_2}\ln\frac{r_\mathrm{e}}{r_\mathrm{s}} + \frac{1}{K_3}\ln\frac{r_\mathrm{f}}{r_\mathrm{e}}\right)\mathrm{d}r_\mathrm{f}(t). \tag{15}$$

The equations of pressure distribution can be derived by substituting equations (9)–(11) into (6)–(8). We could also get the equations of velocity distribution by substituting the pressure equations into (1).

2.2. Heat and Mass Transfer

Using a volume element ΔV, we neglect the different of density between solid and liquid metal. With the hypothesis of instantaneously thermal equilibrium, the heat and mass transfer equations within different regions are presented separately as follows [7].

In region 1, the heat transfer equation could be concluded:

$$\rho_\mathrm{c}c_\mathrm{c}\frac{\partial T}{\partial t} + \rho_\mathrm{m}c_\mathrm{m}u(r,t)\nabla T = \nabla\cdot(\lambda_\mathrm{c}\nabla T) + \rho_\mathrm{m}\Delta H(1 - V_\mathrm{f})\frac{\partial f_\mathrm{s}}{\partial t}. \tag{16}$$

In region 2, the heat transfer equation is:

$$\rho_\mathrm{c}c_\mathrm{c}\frac{\partial T}{\partial t} + \rho_\mathrm{m}c_\mathrm{m}u(r,t)\nabla T = \nabla\cdot(\lambda_\mathrm{c}\nabla T). \tag{17}$$

In region 3, neglected the heat capacity of the gas phase in the preform, we have:

$$\rho_\mathrm{p}c_\mathrm{p}\frac{\partial T}{\partial t} = \nabla\cdot(\lambda_\mathrm{p}\nabla T), \tag{18}$$

where $\rho_\mathrm{p}c_\mathrm{p} = V_\mathrm{f}\rho_\mathrm{f}c_\mathrm{f}$, $\lambda_\mathrm{p} = V_\mathrm{f}\lambda_\mathrm{f}$.

Region 4 is the eutectic region, and for the assumption of the local thermal equilibrium, the temperature is equivalent to the eutectic temperature:

$$T = T_\mathrm{e}, \tag{19}$$

where, $\rho_\mathrm{c}, c_\mathrm{c}, \lambda_\mathrm{c}$ are given by the following equations: $\rho_\mathrm{c} = \rho_\mathrm{f}V_\mathrm{f} + \rho_\mathrm{m}V_\mathrm{m}$; $\rho_\mathrm{c}c_\mathrm{c} = \rho_\mathrm{f}c_\mathrm{f}V_\mathrm{f} + \rho_\mathrm{m}c_\mathrm{m}(1 - V_\mathrm{f})$; $\lambda_\mathrm{c} = \lambda_\mathrm{f}V_\mathrm{f} + \lambda_\mathrm{m}(1 - V_\mathrm{f})$.

In the volume element ΔV, mass transport equation is given by:

$$\frac{\partial C_\mathrm{c}}{\partial t} = -\nabla\big[(1 - V_\mathrm{f})f_\mathrm{L}C_\mathrm{L}u_\mathrm{L}\big], \tag{20}$$

where C_c is given by $C_c = (C_L f_L + C_s f_s)(1 - V_f)$. The relationship between local velocity u_L and superficial velocity u is given by $u_L = u/((1 - V_f) f_L)$.

With the assumption of the straight liquidus line in the alloy phase diagram, the coupling relationship between temperature T and concentration C_L is given by:

$$T - T_m = C_L m_L. \tag{21}$$

2.3. Initial and Boundary Conditions

The initial and boundary conditions are as follows [7]:

Initial conditions, $t = 0$: $r_0 < r < r_1$, $T = T_{m,in}$; $r_1 < r < r_2$, $T = T_{p,0}$.

Boundary conditions:

Boundary $r = r_1$: $P = P_1$, $T = T_{m,in}$.

Boundary 2–3, $r = r_f$: $P_{R2} = P_c, T_{R2} = T_{R3}, f_{R2,s} = 0, \lambda_c \nabla T_{R2} = \lambda_p \nabla T_{R3}, u_{R2} = (1 - V_f) u_{23}$.

Boundary 1–2, $r = r_s$: $T_{R1} = T_{R2} = T_L, C_{R2,L} = C_0, P_{R1} = P_{R2}$,

$$(C_0 - C_{R1,L}) u_{R1} = (C_0 - (1 - (1 - k_0) f_s) C_{R1,L}) u_{12},$$

$$-(\lambda_c (\nabla T_{R2} - \nabla T_{R1})) = \rho_m \Delta H (1 - V_f) f_s u_{12},$$

$$u_{R1} = u_{R2}, \qquad u_{R1} = (1 - V_f)(1 - f_s) u_{12}.$$

Boundary 1–3, $r = r_f$: $P_{R1} = P_c, T_{R1} = T_{R3}, f_{R1,s} = 0, \lambda_c \nabla T_{R1} = \lambda_p \nabla T_{R3}, u_{R1} = (1 - V_f) u_{13}$.

Boundary 1–4, $r = r_e$: $P_{R1} = P_{R4}, T_{R1} = T_{R4} = T_e, C_{R1} = C_{R4} = C_e, f_{R1,s} = 0$,

$$-\lambda_c \nabla T_{R1} = \rho_m \Delta H (1 - V_f) f_{SE} u_{14}.$$

Boundary 4–3, $r = r_f$: $T_{R3} = T_{R4} = T_e, P_{R4} = P_c$,

$$-\lambda_p \nabla T_{R3} = \rho_m \Delta H (1 - V_f) f_{SE} u_{34}, \qquad u_{R4} = (1 - V_f) u_{43}.$$

Boundary $r = r_2$:

$$\rho_p c_p \frac{\partial T}{\partial t} = -\lambda_p \nabla T_{R3}.$$

In the above equations, u_{ij} is the moving velocity of the boundary between region i and j. The subscript Ri means in region i.

3. Model Solutions

3.1. Numerical Solving Process

It is a Stefan problem with multi moving boundaries in different cases for the appearance of different regions. The infiltration front and the boundaries between region 2 and 1, region 1 and 4 are the function of time t.

The relationship between time t and the boundaries' position, such as r_s, r_e, and r_f, are analytically given by (13)–(15). It is important to ascertain the positions of

r_s, r_e, and r_f simultaneously for this problem. In order to simplify the solution, for the one-dimensional problem, the Boltzmann transformation [7] is used to describe the position r_f and t:

$$r_f = \psi\sqrt{t}, \tag{22}$$

where ψ is a variable, but it may not have a definitely value. We also applied the dimensionless parameter $\chi = r/\psi\sqrt{t}$, and another parameter Θ is used to transform temperature T into a dimensionless variable:

$$\Theta = \frac{T_m - T}{T_m - T_L}. \tag{23}$$

By using (22) and (23), the heat transfer equations could be transformed into a function of Θ, χ and ψ. With the heat and concentration coupling function (21), the mass transfer equation (20) could be transformed into a function of Θ, χ, ψ, and f_s. The initial-Boundary models are discretized by using the finite difference method. The concrete solving processes are as following.

An initial location of infiltration front r_f is given to solve this model. ψ is substituted by an assumption ψ_0 at first. At $r = r_f$ ($\chi = 1$), an initial guess of Θ is given to calculate the temperature and concentration fields. Θ at $r = r_f$ will be changed until the Θ solved at $\chi = 0$ is very close to $\Theta_{m,in}$ ($\Theta = \Theta_{m,in} \pm 0.001$). These parameters r_s, r_e could get from the results, then (13)–(15) are used to calculate time t. A new ψ_1 will be derived from (22), then compare ψ_0 and ψ_1 until $|\psi_1 - \psi_0| \leqslant 0.001$. Else, an adjusted ψ_0 is used to repeat the process above. By using this iterative method, we could get the temperature and solute profiles in the end.

3.2. Useful Parameters

The parameters used in simulation are listed in Table 1.

4. Results and Discussion

In the following section, the numerical results are presented to study the influence of various operating parameters, such as inlet metal temperature, initial preform temperature, porosity, and angular velocity on the infiltration process and the solute macrosegregation characteristics.

The temperature, solid volume fraction and average copper solute distributions along the infiltrated region are shown in Fig. 2 for the three cases of the inlet metal temperature: (1) no superheat; (2) small superheat; (3) large superheat. No superheat happens in the inlet metal matrix when $T_{m,in} = T_L$, and the whole infiltrated region contains both solid and liquid phases. With the increment of $T_{m,in}$, the remelting region appears and the length of this region grows rapidly. As shown in the temperature profile of $T_{m,in} = 978$ K, the remelting region occupies more than half the length of the total infiltrated region. The temperature in the mushy region near the infiltration front declines quickly for the chilling effect to the inlet metal

Table 1.
Parameters used in the simulation [5, 8, 9]

Properties	Value	Properties	Value
Specific heat of fiber, c_f (J/(Kg K))	1212.0	Melting temperature of solvent, T_m (K)	933.5
Specific heat of metal, c_m (J/(Kg K))	1179.0	Liquidus temperature, T_L (K)	918.0
Nominal concentration, C_0 (%)	4.5	Surface energy of molten metal, γ (Pa m)	0.893
Eutectic concentration, C_e (%)	32.7	Latent heat of solidification, ΔH (J/Kg)	3.92×10^5
Average diameter of fiber, d_f (m)	3.5×10^{-6}	Contact angle, θ_c (°)	160
Equilibrium partition ratio, k_0	0.173	Thermal conductivity of fiber, λ_f (W/(m K))	35.0
Liquidus slope, m_L (K/wt%)	−3.373	Thermal conductivity of metal, λ_m (W/(m K))	57.3
Radius of initial liquids position, r_0 (m)	5.00×10^{-2}	Density of fiber, ρ_f (kg/m^3)	3300.0
Left boundary position of preform, r_1 (m)	9.00×10^{-2}	Density of metal, ρ_m (kg/m^3)	2983.0
Right boundary position of preform, r_2 (m)	1.20×10^{-1}	Dynamic viscosity, μ (Pa s)	1.2×10^{-3}
Eutectic temperature, T_e (K)	821.2		

caused by the relatively cooler preform. The solid volume fraction in the remelting region is $f_s = 0$, and f_s decreases by increasing $T_{m,in}$ in the mushy region. Fig. 2(b) shows the distribution of the average solute copper concentration. The average concentration in the remelting region is equivalent to the nominal concentration C_0. The enrichment of solute copper occurs mainly at the infiltration front, where C_{av} decreases when a higher $T_{m,in}$ is given. The decrease of C_{av} at the infiltration tip is not remarkable compared to the increase of the length of the remelting region by increasing $T_{m,in}$ from 918 K to 938 K. Large remelting is not available for the high performance of the metal matrix composites, because the presence of remelting region results in coarse columnar grain structure and generates a fairly sharp transition in grain size located to the boundary between remelting and mushy region [10]. So it is not desirable for a high $T_{m,in}$ in order to shorten the remelting region.

The remelting region occupies a larger area and the temperature at the infiltration front is much higher than the eutectic temperature when a larger initial preform temperature is presented, as shown in Fig. 3(a). With the decrement of $T_{p,0}$, the solid volume fraction in the mushy region increase for the enhancive cooling effect of fiber. The eutectic region appears in the infiltration front when the $T_{p,0}$ is decreased. It has a small eutectic region when $T_{p,0} = 723$ K as shown in the curve.

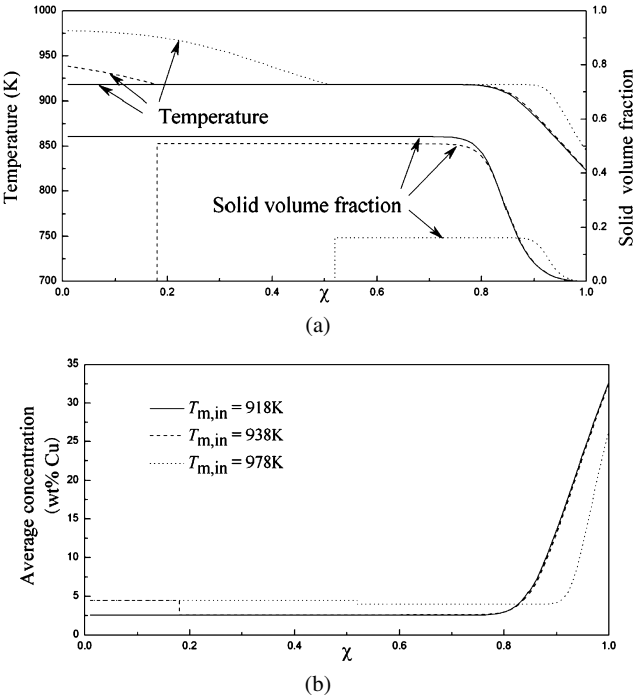

Figure 2. (a) Temperature and solid volume fraction distribution, and (b) average solute distribution under different inlet metal temperatures ($T_{p,0} = 773$ K, $\phi = 0.76$, $\omega = 64\pi$ rad/s).

In the eutectic region, the values of temperature, solid volume fraction, and average concentration are constants: T_e, f_{SE}, C_e. In Fig. 3(b), the average concentration in the remelting region is C_0. The increasing range of the average concentration is gradually increased with the decrement of initial fiber temperature. Considering the decrease of the average concentration at the infiltrtion front, it is better to increase $T_{p,0}$. However, in order to shorten the remelting region and reduce the chemical reactions between the fibers and the metal matrix, the initial fiber temperature is usually lower than the liquidus temperature of metal [11].

The values of the porosity of the preform are given as 0.74, 0.76, and 0.80. Figure 4(a) shows the temperature and solid volume fraction distribution along the infiltrated region under above three different porosities. The value of porosity has a significantly effect to the heat flux through the porous preform. A higher ϕ makes more heat flux through the porous preform, which extends the length of the remelting region by pushing the remelting front and increases the temperature at the infiltration front for stronger heat transfer. The solid volume fraction decreases for large amount heat flux caused by increasing the porosity. As shown in Fig. 4(b), the average copper concentration increases in the front part of the mushy region and reduces at the infiltraion front when a larger porosity is given.

Figure 5 shows the numerical results under different angular velocities. As shown in Fig. 5(a), large remelting region exists in the inlet area when the angular velocity

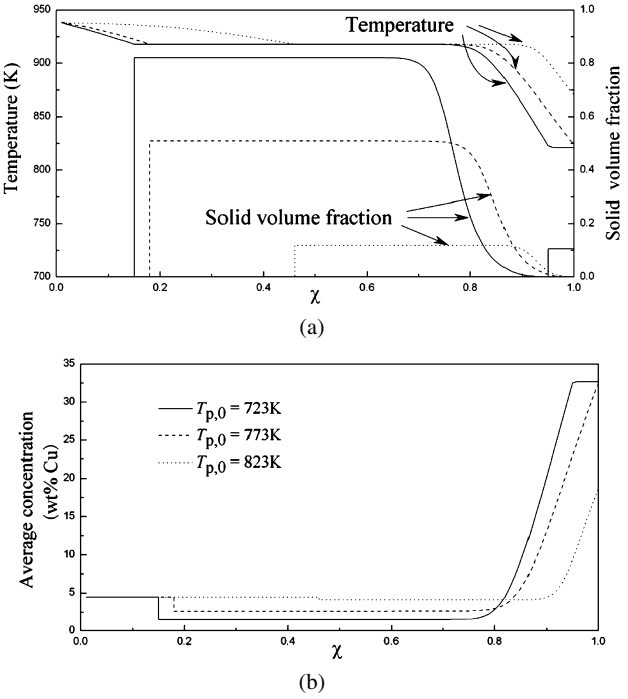

Figure 3. (a) Temperature and solid volume fraction distribution, and (b) average solute distribution under different initial preform temperatures ($T_{m,in} = 938$ K, $\phi = 0.76$, $\omega = 64\pi$ rad/s).

is small, which is because it has enough time for heat transfer in the infiltrated region. With the increment of ω, the temperature at the infiltration front increases gradually and the solid volume fraction turns to much lower in mushy region. The average concentration increases in the front part of the mushy region and reduces at the infiltraion front by increasing the angular velocity as shown in Fig. 5(b). With a higher ω, it can be found that the degree of copper solute enrichment at the infiltration front alleviated. The pressure distributions under different angular velocities are shown in Fig. 6. The pressure distribution curves show an increasing tendency generally along the direction of infiltration when the angular velocity is small, and the pressure at the infiltration front is the maximum P_c. The pressure in the infiltrated region increases significantly when a larger ω is presented. It is concluded that high angular velocity is beneficial to the infiltration advance and reducing the solute enrichment at the infiltration front, but it does not mean that a much higher ω is the better. The pressure at the inner surface of the preform is much bigger with a larger ω, which demands a high strength preform. Therefore, the properties of preform should be considered for the selection of angular velocity.

5. Conclusions

In this article, the influence of different casting conditions are analyzed on the infiltration kinetics and macrosegregation. From the results of the temperature, solid

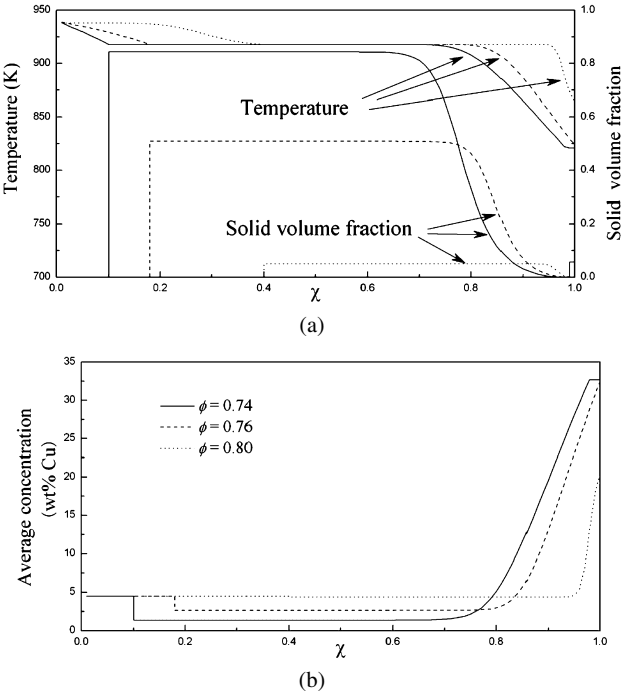

Figure 4. (a) Temperature and solid volume fraction distribution, and (b) average solute distribution under different porosities of preform ($T_{m,in} = 938$ K, $T_{p,0} = 773$ K, $\omega = 64\pi$ rad/s).

volume fraction, average concentration, and pressure profiles, the following conclusions are presented:

1. The mushy region occupies the most area during the liquid alloy infiltrated through the porous preform when superheat is not severe. Remelting region increases obviously and the average concentration at the infiltration front decreases when a larger superheat is given. Less superheat is necessary to shorten the length of the remelting region for the high performance of the composites. Increasing the porosity, initial preform temperature and decreasing the angular velocity tends to enlarge the remelting region.

2. The enrichment of copper concentration is discovered mainly near the infiltration front. High porosity and initial preform temperature incline to alleviate macrosegregation at the tip. In order to reduce the chemical reactions between the fibers and the metal matrix, the initial preform temperature should be lower than the liquidus temperature of alloy.

3. Large angular velocity is favorable to the infiltration advance and reducing the copper solute enrichment at the infiltration front. It also increases the pressure distribution in the infiltrated region significantly, which puts forward a higher requirement for the strength of porous preform. The angular velocity should be selected according the properties of the preform.

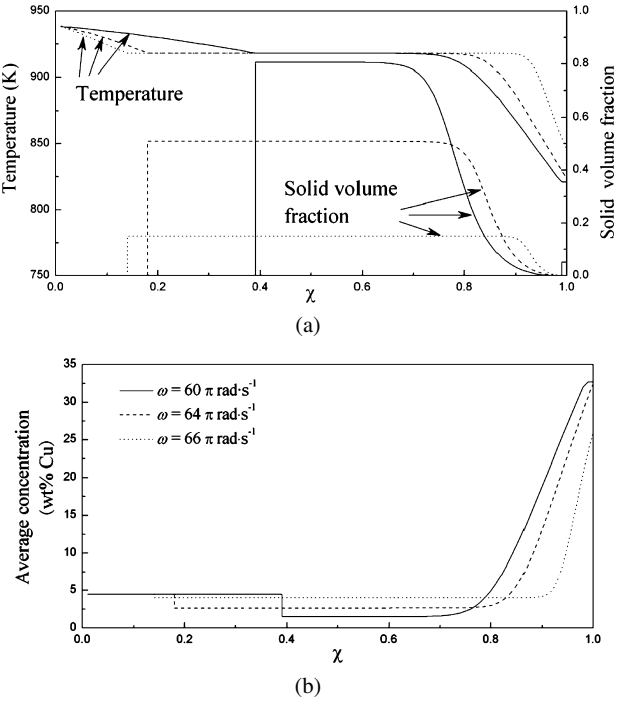

Figure 5. (a) Temperature and solid volume fraction distribution, and (b) average solute distribution under different angular velocities ($T_{m,in} = 938$ K, $T_{p,0} = 773$ K, $\phi = 0.76$).

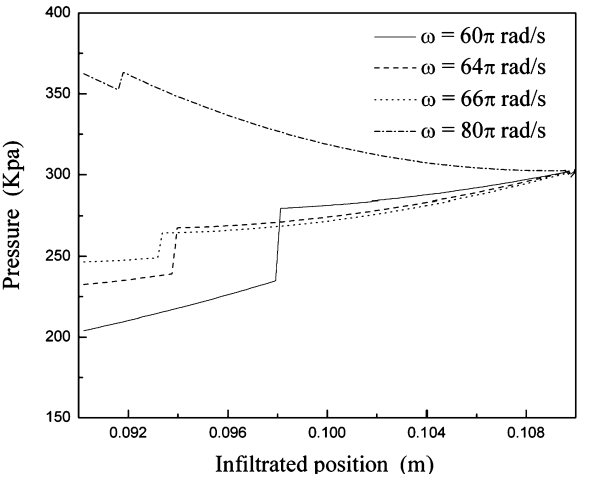

Figure 6. Pressure distribution in the infiltrated region under different angular velocities.

4. Based on the comprehensive consideration of shortening the remelting region and reducing the solute enrichment at the infiltration front, it is clearly scope for optimization of the combination of metal superheat, initial preform temperature, porosity, and angular velocity.

Acknowledgements

The authors gratefully acknowledge the financial support by Doctoral Program Foundation of Institutions of Higher Education of China (No. 20050248021).

References

1. Y. Nishida, I. Shirayanagi and Y. Sakai, Infiltration of fibrous preform by molten aluminum in a centrifugal force field, *Metall. Mater. Trans. A* **27A**, 4163–4169 (1996).
2. M. A. Taha and N. A. El-Mahallawy, Metal-matrix composites fabricated by pressure-assisted infiltration of loose ceramic powder, *J. Mater. Proc. Tech.* **73**, 139–146 (1998).
3. J. Wannasin and M. C. Flemings, Fabrication of metal matrix composites by a high-pressure centrifugal infiltration process, *J. Mater. Proc. Tech.* **169**, 143–149 (2005).
4. D. B. Miracle, Metal matrix composites — from science to technological significance, *Comp. Sci. Tech.* **65**, 2526–2540 (2005).
5. Y. Nishida and G. Ohira, Modelling of infiltration of molten metal in fibrous preform by centrifugal force, *Acta Mater.* **47**, 841–852 (1999).
6. G. X. Hu, Y. H. Li and L. X. Zhang, Solidification and remelting of aluminum though alumina preform under a centrifugal force field, *Scripta Mater.* **56**, 1039–1042 (2007).
7. A. Mortensen and V. Michaud, Infiltration of fiber preforms by a binary alloy: part I. Theory, *Metall. Mater. Trans. A* **21A**, 2059–2072 (1990).
8. Y. Nishida, I. Shirayanagi and Y. Sakai, Infiltration of fibrous preform by molten aluminum in a centrifugal force field, *Metall. Mater. Trans. A* **27A**, 4163–4169 (1996).
9. A. V. Reddy and C. Beckermann, Modeling of macrosegregation due to thermosolutal convection and contraction-driven flow in direct chill continuous casting of an Al–Cu round ingot, *Metall. Mater. Trans. B* **28B**, 479–489 (1997).
10. T. W. Clyne and J. F. Mason, The squeeze infiltration process for fabrication of metal-matrix composites, *Metall. Mater. Trans. A* **18A**, 1519–1530 (1987).
11. A. Cantarel, E. Lacoste, M. Danis and E. Arquis, Metal matrix composite processing: numerical study of heat transfer between fibers and metal, *Int. J. Numer. Methods Heat Fluid Flow* **15**, 808–826 (2005).